Investigation on Viscosity and Non-isothermal Crystallization Behavior of P-bearing Steelmaking Slags with varying TiO_2 Content

Zhanjun WANG[1)], Yongqi SUN[2)], Seetharaman SRIDHAR[3)], Mei ZHANG[1)], and Zuotai ZHANG[4)*]

1) School of Metallurgical and Ecological Engineering, University of Science and Technology Beijing, 100083, Beijing, P.R. China

2) College of Engineering, Peking University, 100871, Beijing, P.R. China

3) Advanced Steel Research Centre, WMG, Steels Processing Research Centre, University of Warwick, Coventry CV4 7AL, UK

4) School of Environmental Science and Engineering, South University of Science and Technology of China, 518055, Shenzhen, P.R. China

*Corresponding author: zhangzt@sustc.edu.cn

ABSTRACT

The viscous flow and crystallization behavior of CaO-SiO_2-MgO-Al_2O_3-Fe_tO-P_2O_5-TiO_2 steelmaking slags have been investigated over a wide range of temperatures under Ar (High purity, >99.999%) atmosphere, and the relationship between viscosity and structure was determined. The results indicated that the viscosity of the slags slightly decreased with increasing TiO_2 content. The constructed non-isothermal continuous cooling transformation (CCT) diagrams revealed that the addition of TiO_2 lowered the crystallization temperature. This can mainly be ascribed to that addition of TiO_2 promotes the formation of $[TiO_6]$-octahedra units, and consequently the formation of $MgFe_2O_4$-Mg_2TiO_4 solid solution. Moreover, the decreasing viscosity has a significant effect on enhancing the diffusion of ion units, such as Ca^{2+} and $[TiO_4]$-tetrahedra, from bulk melts to crystal-melt interface. The crystallization of $CaTiO_3$ and $CaSiTiO_5$ was consequently

accelerated, which can improve the phosphorus content in P-enriched phase (n2CaO·SiO_2-3CaO·P_2O_5). Finally, the non-isothermal crystallization kinetics was characterized and the activation energy for the primary crystal growth was derived that the activation energy increases from -265.93 KJ·mol^{-1} to -185.41 KJ·mol^{-1} with the addition of TiO_2 content, suggesting that TiO_2 lowered the tendency for the slags to crystallize.
Key words: Steelmaking slags, TiO_2, Viscosity, Kinetics, Structure

1. INTRODUCTION

The production of crude steel in China surpassed 800 million tons in 2015, disposing nearly 80 to 100 million tons of steelmaking slags.[1] However, only about 30wt.% of steelmaking slags were recycled as construction materials, soil conditioners, fertilizers, recovery of metals or recovered in iron- and steelmaking process, *etc*.[2-7] Among these utilization methods, the most effective way of utilizing the steelmaking slags was recycled into the iron- and steelmaking process, which may inevitably result in the enrichment of phosphorus in the slags and further increase the burden in the following dephosphorization process.[8-10] Thus, the lowering of the phosphorus content in steelmaking slags is of primary concern for further utilization of P-bearing steelmaking slags. The selective crystallization and phase separation (SCPS) method has been proved to be the most efficient way to recycle the phosphorous in steelmaking slags.[11-13] During the SCPS process, the selective crystallization is the key step to successfully enrich phosphorous into a certain phase, which can be separated and used as phosphorus fertilizer, and the residues may be recycled into iron- and steelmaking process.

During the early 1960 and 1980s, a number of investigations have been conducted to detect the dephosphorization process.[14-17] These investigations were mainly based on CaO-SiO_2-Fe_tO-P_2O_5 system to study the mechanism of dephosphorization, and the n(2CaO·SiO_2-3CaO·P_2O_5) ($n$$C_2S$-$C_3P$) solid solution has been considered as the efficient P-enriched phase. Based on these investigations,

various studies have been explored to reveal how to boost the phosphorus content in $n$$C_2S$-$C_3P$ solid solution through adding different additives in the complex CaO-SiO_2-MgO-Al_2O_3-Fe_tO-P_2O_5 multiphase.[9,18-21] A series of studies have been carried out to explore the P concentrating phase in steelmaking slags modified by Fe_2O_3, P_2O_5, Al_2O_3 and CaF_2 additives,[22-25] where the essential structure of the slags has been systematically studied, especially Fe^{3+}, P^{5+}, Al^{3+} and F^-. Meanwhile, some other studies about the structure also replenished the investigation of the slags.[26-29] However, the existing data is still too limited to cover all of the slag compositions. Some studies showed that TiO_2 can also be used as an additive to improve P (or V) solid solubility in the P (or V)-enriched phase,[19,30] during which process the viscosity and crystallization ability changed correspondingly. It is well known that Ti^{4+} can act as a network former cation with fourfold coordination of oxygen or a network modifier cation with sixfold coordination of oxygen, the effect of TiO_2 on enrichment of phosphorus was strongly needed for systematical extrapolation to expand the previous experimental data.

The objective of the present study was to provide a comprehensive exploration and discussion of CaO-SiO_2-Al_2O_3-MgO-Fe_tO-P_2O_5 slags modified by TiO_2 with the content range from 0 to 10 wt.%, including the variation of viscosity and structure of the melts, the precipitation sequence of the crystals, and the kinetics of the primary crystals during the continuous cooling.

2. EXPERIMENTAL

The raw materials of the synthetic slags were analytical grade CaO, SiO_2, MgO, Al_2O_3, Fe_2O_3, P_2O_5 and TiO_2. The samples were prepared at 1823 K under 0.3L/min of Ar (High purity, >99.999%) in a platinum crucible to obtain the homogeneous slags for two hours. The molten slags were then quenched into water rapidly and crushed for the primary experiments. The quenched slags were examined by X-ray diffraction (XRD) to insure the glassy phase, as shown in **Figure 1**. The chemical compositions of the pre-melted slags for the current study were analyzed by X-ray fluorescence

(XRF), as shown in **Table 1**, where $Fe^{3+}/\sum Fe$ were determined by the titration method. Additionally, the equilibrium state of the molten slag can be achieved when the holding time was beyond two hours. It can be clarified through the constant $Fe^{3+}/\sum Fe$ values. It is therefore reasonable concluded that the pre-melted slags with the holding time for two hours can be used for further measurement.

The viscosity measurement was carried out by rotating cylinder method using a rotating spindle connected to a calibrated Brookfield digital viscometer (*model LVDV-II+, Brookfield Engineering Laboratories, Middleboro, MA*). The experimental apparatus for the viscosity measurement and the other details of the experimental apparatus can be found in our previous study.[25,31] Within the scope of the viscosity measurement, although the oxygen partial pressure around the Mo crucible was low enough, the Mo crucible was inevitably oxidized as MoO_x. The MoO_x contents after the viscosity was less than 0.71wt.% and the change before and after the viscosity measurement is less than 0.32 wt.%. Therefore, the effect of MoO_x can be ignored during the viscosity measurement.

The non-isothermal melt crystallization of the slags were evaluated with differential scanning calorimeter (DSC) by a SETARAM instrument (*Setsys Evolution, S60/58341, SETARAM Instrumentation, France*) in Ar atmosphere (Ar purity >99.999%) at a flow rate of 60 ml/min with α-Al_2O_3 as the reference. Before the DSC experiment, the instrument calibration was performed using high purity metals of Al, Ag, Au and Ni. Then, about 40 mg slags were heated up at a constant heating rate of 20K/min in a platinum crucible with a diameter of 5 mm and a height of 8 mm. The molten slags were held at 1823 K for 5 minutes to homogenize the chemical composition. Subsequently, the slags were cooled at different cooling rates (5, 10, 15, 20, and 25 K/min). Furthermore, the baseline was employed to calibrate the DSC curves for the buoyancy effect.

Since the molten slags after DSC measurements are too small to identify the crystal phases by XRD and SEM, a series of heat treatment experiments were carried out in order to determine the sequence of crystalline phase precipitation. First of all, the previous pre-melted slags were heated to 1823K and cooled to the target

temperature at a cooling rate of 10 K/min. Afterwards the slags were held about 30 minutes at each target temperature and then quenched by water. The crystals in slags were identified by X-ray diffraction (XRD) and the scanning electronic microscopy equipped with energy dispersed spectroscopy (SEM/EDS).

A more quantitative analysis of structure can be obtained by using Raman spectra performed with a multichannel modular triple Raman system (*JY-HR800, Jobin-Yvon, France*) with excitation wavelength of 532 nm and a 1 mW semiconductor laser as the light source. Solid-state ^{29}Si MAS-NMR measurements of the power glasses were recorded on a 400 M FT-NMR spectrometer (*Bruker Avance III 400M, Germany*) using a MAS probe with 4 mm ZrO_2 rotor and two pairs of Dupont Vespel caps.

3 RESULTS

A. Viscosity measurement

The effect of TiO_2 addition on the viscosity of the typical basic oxygen $CaO\text{-}SiO_2\text{-}Al_2O_3\text{-}MgO\text{-}Fe_tO\text{-}P_2O_5$ steelmaking slags at a fixed CaO/SiO_2 ratio of 1.8 is shown in **Figure 2**. It can be noted that the slag viscosity decreases with increasing TiO_2 content. In spite of different slag compositions investigated, the variation trend of present result is in good agreement with the previous results. Zheng *et al*.[31] have investigated the effect of TiO_2 addition on the viscosity of $CaO\text{-}SiO_2\text{-}TiO_2$ (C/S=1.2) slags, and found that the viscosity of these ternary slags decreased with an increment in the content of additive TiO_2. Park *et al*.[32] reported that TiO_2 behaved as the basic oxide and lowered the viscosity in the $CaO\text{-}SiO_2\text{-}Al_2O_3\text{-}MgO$-based slags by depolymerizing the silicate network structure. Wang *et al*.[33] examined the effect of TiO_2 addition on the viscosity of $CaO\text{-}SiO_2\text{-}Al_2O_3\text{-}MgO\text{-}Na_2O\text{-}B_2O_3$ system in the temperature range of 1583 K to 1448 K and obtained the similar variation trend. Furthermore, the relative viscosity reported by present study is lower than that of previous investigations, which can be ascribed to the higher basicity and more complex multiphase in the present study.

B. DSC investigation

The DSC investigation of the studied slags was inquired under non-isothermal conditions at five cooling rates. **Figure 3** records the DSC curves of the slags with different TiO_2 contents during continuous cooling process at cooling rates of 5, 10, 15, 20 and 25 K/min, respectively. According to Jung *et al*.,[26] each separate peak suggested a discrete crystallization of different phases during cooling process. The starting point of the crystallization (onset temperature, T_{onset}) was taken from the intersection between the tangent line of the heat flow curve before the exothermic peak and the tangent line of the steep exothermic peak curve, as shown in **Figure 3** (a). At all the considered cooling rates, the DSC curves of slag 1 have the similar shapes, *i.e*., four DSC exothermic peaks were obtained in **Figure 3** (a). The peaks were denoted as P1, P2, P3 and P4 for slag 1, corresponding to four different crystallization events occurred in slag 1 under different continuous cooling rates.[34] However, it was observed that there were five exothermic peaks for slags containing TiO_2, indicating the occurrence of a new crystallization event in the slag with TiO_2 additions. For the TiO_2 containing slags, the peaks were designated as P1, P2, P3, P4, and P5, respectively. Comparing the position of exothermic peaks on DSC curves at the cooling rate of 5K/min, a significant shift occurred toward a lower temperature and shape of exothermic peaks became sharper with increasing cooling rate. Clearly, crystallization parameters such as nucleation and growth rates are functions of viscosity and degree of undercooling. Therefore, at a higher cooling rate, a higher undercooling was required and a lower crystallization temperature was caused.

Based on the aforementioned results, the CCT diagrams for the primary crystals with varying TiO_2 contents were constructed. It can be seen from **Figure 4** that the crystallization temperature decreases with increasing TiO_2 contents in the slags, which suggests that TiO_2 lowers the tendency of crystallization. This result is not completely consistent with the previous results. For instance, Wen *et al*.[35] found that the crystallization ability of $CaO\text{-}SiO_2\text{-}TiO_2$ systems increased first with increasing TiO_2 content, while the crystallization was restrained with further addition of TiO_2 content.

The difference of the crystallization ability can be ascribed to the complex system and the multiple identities of Ti^{4+} (network modifier or network former). Therefore, the effect of TiO_2 on crystallization can be further elucidated in following sections.

C. Identification of the Crystal Phases

In order to determine the crystal phases associated with the exothermic peaks appearing in the non-isothermal DSC curves, the slag 1 and slag 3 were heat treated to qualitative characterize the behavior of crystallization. The slags were melted at 1823 K, and then continuously cooled at the cooling rate of 10 K/min to the desired temperatures. At each desired temperature, the melts would be held 30 minutes isothermally to ensure that the crystal grew to a sufficient size for further characterization, and were then extracted and quenched in water. The as-quenched slags were analyzed by XRD and the patterns obtained are shown in **Figure 5**. It can be seen that $MgFe_2O_4$ spinel is the first crystal to precipitate upon cooling for slag 1 at 1473 K, followed by $MgFe_2O_4$ and *n*C_2S-C_3P that co-precipitated at 1413 K, indicating that the exothermic peaks P1 and P2 represented the precipitation of spinel ($MgFe_2O_4$) and P-enrich phase (*n*C_2S-C_3P), respectively. Unlike slag 1, with increasing TiO_2 content, it can be seen from **Figure 5** (b) that the first crystalline phase is transformed to the mixture of $MgFe_2O_4$ and Mg_2TiO_4. The second exothermic peak P2 still signifies the formation of P-enriched phase. In addition, it can be seen from the XRD patterns of slag 3 quenched at 1173K that $CaTiO_3$ and Ca_2TiSiO_4 can be detected, which can also be interpreted by phase diagram of CaO-SiO_2-TiO_2 system.[36] It can be seen from the CaO-SiO_2-TiO_2 phase diagram that the thermodynamic condition was favorable to the formation of $CaTiO_3$ and Ca_2TiSiO_4 at a higher TiO_2 content. For P-bearing slags, the enhancement of $CaTiO_3$ and Ca_2TiSiO_4 formation further promoted the enrichment of phosphorus into a certain phase (n'C_2S-C_3P, n>n'), which would be formulated by the following equation.[19]

$$n\mathrm{Ca_2SiO_4 \cdot Ca_3(PO_4)_2} + \mathrm{TiO_2} \rightarrow \mathrm{CaSiTiO_5} + \mathrm{CaTiO_3} + n'\ \mathrm{Ca_2SiO_4 \cdot Ca_3(PO_4)_2}$$

(1)

To clarify the XRD results and the morphologies of the crystalline phases, SEM/EDS technique was employed to display the different types of phases. **Figure 6** and **Table 2** show the back-scatter electron microscopy of the slags with TiO_2 additions of 0, 5 and 10wt.%, respectively. It can be seen from **Figure 6** (a) and (b) that, for slag 1, the first precipitated granular pale crystal can be identified as spinel ($MgFe_2O_4$) and the following precipitated polygonal grey crystal can be determined as P-enriched phase ($n$$C_2S$-$C_3P$), respectively. It is worthy to note that the inner part of the polygonal grey crystal (phase C, **Figure 6** (b)) can be identified as $2CaO{\cdot}SiO_2$. Further consideration about $n$$C_2S$-$C_3P$ crystallization behavior and its mechanism would be meaningful. Compared with the previous study, the precipitation mechanism for the P-enriched phase can be elucidated here:[37] first, $2CaO{\cdot}SiO_2$ particle precipitated from the molten slag; second, P_2O_5 and CaO around the $2CaO{\cdot}SiO_2$ particle diffused to $2CaO{\cdot}SiO_2$ surface quickly; third, P_2O_5 existed as $3CaO{\cdot}P_2O_5$ and diffused into the $2CaO{\cdot}SiO_2$ particle and the composition of the particle changed to $5CaO{\cdot}SiO_2{\cdot}P_2O_5$. As demonstrated in **Figure 6** (c), for slag 3, the primary crystal transformed to the white lumps. These white lumps cannot be distinguished clearly through the appearance of the crystal, but when combining the image with the XRD and EDS results, the white lumps may be explained as solid solution of $MgFe_2O_4$-Mg_2TiO_4.[38] Furthermore, some other information can also be concluded from the EDS and XRD result that the Fe-enriched phase ($MgFe_2O_4$) and P-enriched phase ($n$$C_2S$-$C_3P$) behaved as the first two precipitated phase during the continuous cooling process.

4. DISCUSSION

A. Non-isothermal Crystallization Kinetics

With the wide use of differential scanning calorimeter (DSC) at crystallization study, several methods have been put forward to obtain kinetic parameters from non-isothermal experiments carried out at different cooling rates.[39-41] During the

non-isothermal crystallization process, the relative degree of crystallinity can be determined by measuring the partial area of DSC peak. The relative degree of crystallinity α as a function of relative crystallization time can be theoretical estimated by means of the following equation: [42]

$$\alpha = \frac{\int_{t_0}^{t}(dH_t/dt)dt}{\int_{t_0}^{t_1}(dH_t/dt)dt} \qquad (2)$$

where dH_t is the measured enthalpy of crystallization during an infinitesimal time interval dt in DSC measurement, t_0 is the time at which the crystallization just begins, and t_1 is the time when the crystallization is completed. **Figure 7 (a)** depicts the relative degree of crystallinity for primary crystal of slag 1 at five different cooling rates, which showed the S-shape curves. It is obviously observed that the t_1 value decreased with increasing cooling rate, suggesting that the crystal grew faster when the cooling rate increased. In addition, the S-shape curves can be schematically divided into three regions, *i.e.*, the random nucleus of crystal occurring at stage A, then the crystal growing rapidly at stage B and the coalescence of crystal happening at stage C.[41] **Figure 7 (b)** shows the crystallization time of primary crystals with the cooling rate of 10K/min. Compared with slag 1, it can be seen that the crystallization time of P1 for slag 2 with 3wt.% TiO_2 has a slightly decrease. This may be attributed to the lower viscosity accelerating the mass transfer. However, with the addition of TiO_2 above 3wt.%, the primary crystal phase is transformed to $MgFe_2O_4$-Mg_2TiO_4 solid solution. Therefore, the content of the formed solid solution increased with increasing TiO_2 content, resulting the crystallization time of $MgFe_2O_4$-Mg_2TiO_4 increased.

The effect of TiO_2 on the crystallization of the slags was further analyzed by calculating activation energy of crystal growth, which is one of the most important kinetic parameters for crystallization process. By taking into account the influence of various cooling rate, Kissinger proposed a method for determining the activation energy values based on the first exothermic crystallization peaks.[39] In this study, the activation energy E_a could be determined by calculating the variation of the crystallization peak temperature with the cooling rate. The equation was shown as

follows:[39]

$$\ln\left(\frac{\beta}{T_p^2}\right) = -\frac{E_a}{RT_p} + \ln(\frac{AR}{E_a}) \qquad (3)$$

where T_p is the maximum crystallization temperature in a DSC curve, β is the cooling rate, R is universal gas constant, and A is frequency factor, respectively. Because the dependence of $\ln(\beta/T_p^2)$ *vs.* $1/T_p$ at considered temperatures is evidently a straight line, it is possible to evaluate the corresponding values of E_a using equation (3). Combining with the slope of the lines, the values of activation energy was calculated and labeled in **Figure 8**. It has been assumed in some works that the activation energy can reflect the tendency of the slag to crystallize, *i.e.*, a higher activation energy value means a bigger barrier to form ordered structures.[43] It can be seen from **Figure 8** that, as TiO_2 content increase from 0 to 10 wt.%, there is a noticeable increase on the activation energy for crystal growth. It suggested that TiO_2 lowers the tendency for the slags to crystallize, which is consistent with the CCT diagrams, *i.e.*, a higher TiO_2 content caused a lower crystallization temperature.

B. Structural Analysis

Generally, the structure characteristic of the slags is closely related to the viscosity and further the crystallization behavior. Therefore, Raman and NMR spectra were employed to detect a clear view of the influence of TiO_2 on the relationship between the viscosity and the crystal formation.

Figure 9 exhibits the deconvoluted Raman spectra of slag 1, 3 and 5, which fitting process was conducted under the guidance of the study performed by Mysen.[44] The previous study assigned the bands at about 855, 920, 988 and 1050 cm^{-1} to the presence of Q^0, Q^1, Q^2 and Q^3 units (Q^n, n=NBO/Si, NBO is the non-bridging oxygen number), respectively. In addition, the peaks near 970 cm^{-1} and 1100 cm^{-1} correspond to the vibration of the dominant P-related groups, *i.e.*, P-O-P and Si-O-P in the structure. The band near 680cm^{-1} can be assigned to the tetrahedrally coordinated Fe^{3+}.[25-26] By analogy with the spectroscopic results on the melts with others,[31,45] the

bands at about 790 cm^{-1} and 845 cm^{-1} can be assigned to $Ti_2O_6^{4-}$ chain units and TiO_4^{4-} monomers (or Si-O-Ti) structural units, respectively. The band around 644 cm^{-1} could be ascribed to Ti-O stretch vibration of Ti^{4+} in [TiO_6]-octahedra. Additionally, the band in the vicinity of 710 cm^{-1} probably is due to O-Ti-O or O-(Si,Ti)-O deformation in chain or sheet units or both.[45-46]

It can be found from the deconvoluted Raman spectra that with the increasing TiO_2 content, the Q^2 and Q^3 bands gradually increase in intensity and become more distinct, while the intensity of Q^0 and Q^1 bands decrease. It means the increasing degree of the polymerization (DOP) of the silicate structure. According to Mysen,[47] the role of TiO_2 can compete with silicate complexes to coordinate metal cations (such as Ca^{2+}). The competition process can be represented by the following reaction:[45-46]

$$Si-O-M-O-Si + Ti-O-Ti \rightarrow Si-O-Si + Ti-O-M-O-Ti \quad (4)$$

$$Si-O-M + Ti-O-Ti \rightarrow Si-O-Ti + Ti-O-M \quad (5)$$

where M represents the metal cation. Therefore, some portion of the non-bridging oxygens in the silicate melts transformed to bridging oxygen with the addition of TiO_2, thereby polymerizing the portion of the silicate network, which can also be validated from the ^{29}Si NMR as shown in **Figure 10**. Furthermore, Ti^{4+} can substitute for Si^{4+} in tetrahedral coordination in the structural units in the structure and the number of average bridging oxygen will be significantly larger. In this case, the DOP of the slags will be increased in theory.

However, the physical properties of silicate melts such as viscosity are dependent on both the degree of polymerization and the strength of oxygen bridges in the silicate melts.[45] The present structural study shows that the degree of polymerization is slightly enhanced with TiO_2 addition. Therefore, the decreasing viscosity could not be explained by the increasing DOP. According to Zhang *et al*.[47] and Zheng *et al*.,[31] the strength of Ti-O bonds seems to be much weaker than Si-O bonds for the reason that Ti^{4+} cation is larger in size and smaller in electronegativity comparing with Si^{4+}, thus addition of TiO_2 to highly polymerized melts will decrease the viscosity.

Additionally, from the viewpoint of structure, the Ti-related bands could give a qualitative explanation to the change of crystal phases, especially Mg_2TiO_4, $CaTiO_3$ and $CaSiTiO_5$. According to Grave[49] and Ye[50], Ti^{4+} was octahedrally coordinated in Mg_2TiO_4. Harrison *et al*.[38] investigated the cation ordering of $MgFe_2O_4$-Mg_2TiO_4 solid solution and found the dominant chemical interaction of the solid solution was a positive nearest-neighbor pairwise interaction between tetrahedrally coordinated Fe^{3+} and octahedrally coordinated Ti^{4+}. Therefore, $[FeO_4]$-tetrahedra and $[TiO_6]$-octahedra can copolymerize to expedite the $MgFe_2O_4$-Mg_2TiO_4 solid solution formation, which has a lower crystallization temperature in thermodynamics. In addition, the $[TiO_6]$-octahedra structure unit is also the main component to build structure of $CaTiO_3$.[51] Therefore, $CaTiO_3$ was gradually crystallized. According to Li[51] and Kirkpatrick[52], $CaTiO_3$ crystals were in non-faceted morphology and the crystallization rate of $CaTiO_3$ rate was controlled by the diffusion of ion units (Ca^{2+} ion and octahedrally coordinated Ti^{4+} units) from bulk melts to crystal-melt interface. In this case, the decreasing viscosity has a constructive effect on the crystallization of $CaTiO_3$. Moreover, the appearance of Ti-O-Si band characterized that the $[TiO_4]$-tetrahedra units can copolymerize with $[SiO_4]$-tetrahedra units to enhance the crystallization of $CaSiTiO_5$.

Combining the microstructure with the crystallization analysis, the primary enrichment mechanism of phosphorus may be elucidated. As the chemical equation (1) shows in Section 3, TiO_2 would capture C_2S (Ca^{2+} and $[SiO_4]$ units) from the early precipitated solution ($n$$C_2S$-$C_3P$) to form $CaSiTiO_5$ and $CaTiO_3$, *i.e.*, C_2S vanished gradually (which can also be clarified from the decreasing Q^0 unit in Raman and NMR spectra[53]) and improved the concentration of phosphorus in P-enriched phase, which is in consistent with the result of XRD. Moreover, it can be found form **Table 2** that the solid solubility of phosphorus in P-enriched phase can reach a high value as 30.17 wt.% which can fully reach the phosphorus content requirements of phosphatic fertilizer for agriculture.

5. CONCLUSION

In the present study, the effect of TiO_2 on the viscous and crystallization behavior of P-bearing steelmaking slags was investigated. The results can be summarized as follows:

The viscosity of the slags decreased with increasing TiO_2 content and the crystallization tendency also decreased with the addition of TiO_2. Additionally, an increasing TiO_2 content promotes the formation of $[TiO_6]$-octrahedra units, which are octahedrally coordinated in $MgFe_2O_4$-Mg_2TiO_4 solid solution and $CaTiO_3$. Moreover, $[TiO_4]$-tetrahedra units can copolymerize with $[SiO_4]$-tetrahedra to form $CaSiTiO_4$. It's meaningful to find that the formation of $CaTiO_3$ and $CaSiTiO_4$ were beneficial to the enrichment of phosphorus in the P-enriched phase, which enhanced the solid solubility of phosphorus in the P-enriched phase by removing units of $2CaO{\cdot}SiO_2$ and thus increasing the P-content in $n2CaO{\cdot}SiO_2$-$3CaO{\cdot}P_2O_5$.

ACKNOWLEDGMENTS

Supports by the National Natural Science Foundation of China (51522401, 51472007, 51372019), and National High Technology Research and Development Program of China (863 Program, 2012AA06A114) are acknowledged.

REFERENCES

1. World steel association: https://www.worldsteel.org/media-centre/press-releases/2015/World-crude-steel-output-increases-by-1.2--in-2014.html.
2. B. Das, S. Prakash, P. Reddy, and V. Misra: *Resour. Conserv. Recy*., 2007, vol. 50, pp. 40-57.
3. M. Shi, Q. Wang, and Z. Zhou: *Constr. Build. Mater*., 2015, vol. 98, pp. 649-655.
4. Q. Wang, M. Shi, and Z. Zhang: *J. Therm. Anal. Calorim.*, 2015, vol. 120, pp. 1241-1248.
5. P. Yan, G. Mi, and Q. Wang: *J. Therm. Anal. Calorim.*, 2014, vol. 115, pp.193-200.
6. Q. Wang, J. Yang, and P. Yan: *Powder Technol*., 2013, vol. 245, pp.35–39.
7. Q. Wang, P. Yan, and J. Yang: *Constr. Build. Mater*., 2013, vol. 47, pp. 1414-1420.
8. J. Jun: *Min. Metall*., 2003, vol. 12, pp. 33-37.
9. L. Lin, Y.P. Bao, M. Wang, and H.M. Zhou: *Ironmak. Steelmak*., 2014, vol. 41, pp. 193-198.
10. L. Lin, Y.P. Bao, M. Wang, W. Jiang, and H.M. Zhou: *J. Iron Steel Res. Int.*, 2014, vol. 21, pp. 496-502.
11. M.Y. Wang, L.N. Zhang, L. Zhang, Z.T. Sui, and G.F. Tu: *Trans. Nonferrous Met. Soc. China*, 2006, vol. 16, pp. 421-425.
12. X.R. Wu, J.N. An, R.H. Chen, and L.S. Li: *J. Anhui Univ. Tech*., 2010, vol. 27, pp. 233-237.
13. Y.Q. Sun, J. Li, X.D. Wang, and Z.T. Zhang: *Metall. Mater. Trans. B*, 2014, vol. 45, pp. 1446-1455.
14. G. Kor: *Metall. Mater. Trans. B*, 1977, vol. 8, pp. 107-113.
15. H. Suito and R. Inoue: *Trans. ISIJ*, 1982, vol. 22, pp. 869-877.
16. J. Berak and I. Tomczakh: *Roczniki Chemii*, 1972, vol. 46, pp. 2157-2164.
17. H. Ono, A. Inagaki, T. Masui, H. Narita, S. Nosaka, T. Mitsuo, and S. Gohda:

Trans. ISIJ, 1981, vol. 21, pp. 135-144.

18. L. Lin, Y.P. Bao, Q. Yang, M. Wang, and W. Jiang: *Ironmak. Steelmak*., 2015, vol. 42, pp. 331-338.
19. L. Lin, Y.P. Bao, M. Wang, and H.M. Zhou: *J. Univ. Sci. Technol. Beijing*, 2014, vol. 36, pp. 1013-1019.
20. L. Jiang, J. Diao, X. Yan, B. Xie, Y. Ren, T. Zhang, and G. Fan: *ISIJ Int.*, 2015, vol. 55, pp. 564-569.
21. J. Diao, B. Xie, Y.H. Wang, and X. Guo: *ISIJ Int.*, 2010, vol. 50, pp. 768-770.
22. Z.J. Wang, Y.Q. Sun, S. Sridhar, M. Zhang, M. Guo, and Z.T. Zhang: *Metall. Mater. Trans. B*, 2015, vol.46, pp.537-541.
23. Z.J. Wang, Y.Q. Sun, S. Sridhar, M. Zhang, M. Guo, and Z.T. Zhang: *Metall. Mater. Trans. B*, 2015, vol. 46, pp. 2246-2254.
24. Z.J. Wang; Y.Q. Sun, S. Sridhar, M. Zhang, M. Guo, Z.M. Li, Z.C. Guo, and Z.T. Zhang: *ISIJ Int*., 2016, vol. 56, pp. 546-553.
25. Z.J. Wang, Q.F. Shu, S. Sridhar, M. Zhang, M. Guo, and Z.T. Zhang: *Metall. Mater. Trans. B*, 2015, vol. 46, pp. 758-765.
26. S.S. Jung and I. Sohn: *Environ. Sci. Technol*., 2014, vol. 48, pp. 1886-1892.
27. Y.B. Cheng, C. Xu, S.Y. Pan, Y.F. Xia, R.C. Liu, and S.X. Wang: *J. Non-Cryst. Solids*, 1986, vol. 80, pp. 201-208.
28. A. Tilocca and A.N. Cormack: *J. Phys. Chem. B*, 2007, vol. 111, pp. 14256-14264.
29. J.L. Li, Q.F. Shu and K.C. Chou: *ISIJ Int*., 2014, vol. 54, pp. 721-727.
30. L.S. Li, X.R. Wu, L. Yu, and Y.C. Dong: *Ironmak. Steelmak*., 2008, vol. 35, pp. 367-370.
31. K. Zheng, Z.T. Zhang, L.L. Liu and X.D. Wang: *Metall. Mater. Trans. B*, 2014, vol.45, pp.1-9
32. H. Park, J.Y. Park, G.H. Kim, and I. Sohn: *Steel Res. Int.*, 2012, vol. 83, pp. 150-156.
33. Z. Wang, Q.F. Shu, and K.C. Chou: *Steel Res. Int.*, 2013, vol. 84, pp. 766-776.
34. M.D. Seo, C.B. Shi, J.W. Cho, and S.H. Kim: *Metall. Mater. Trans. B*, 2014, vol.

45, pp. 1874-1886.

35. G.H. Wen, S. Sridhar, P. Tang, X. Qi and Y.Q. Liu: *ISIJ Int*., 2007, vol. 47, pp. 1117-1125.
36. V. D. Eisenhüttenleute. *Slag atlas*. *Verlag Stahleisen*, 1995.
37. S. Fukagai, T. Hamano, and F. Tsukihashi: *ISIJ Int*., 2007, vol. 47, pp. 187-189.
38. R.J. Harrison, E.J. Palin, and N. Perks: *Am. Mineral.*, 2013, vol. 98, pp. 698-708.
39. H.E. Kissinger: *J. Res. Natl. Bur. Stand.*, 1956, vol. 57, pp. 217-221.
40. T. Ozawa: *Polymer*, 1971, vol. 12, pp. 150-158.
41. S. Haratian and M. Haddadsabzevar: *J. Non-Cryst. Solids*, 2015, vol. 429, pp.164-170.
42. P. Supaphol, N. Dangseeyun, P. Srimoaon, and M. Nithitanakul: *Thermo. Acta*, 2003, vol. 406, pp. 207-220.
43. M. Dapiaggi, G. Artioli, C. Righi, and R. Carli: *J. Non-Cryst*, 2007, vol. 353, pp. 2852-2860.
44. B.O. Mysen, L.W. Finger, D. Virgo, and F.A. Seifert: *Am. Mineral.*, 1982, vol. 67, pp. 686-695.
45. B.O. Mysen: *Am. Mineral.*, 1980, vol. 65, pp. 1150-1165.
46. S.F. Zhang, X. Zhang, C.G. Bai, L.Y. Wen, and X.W. Lv: *ISIJ Int*., 2013, vol. 53, pp. 1131-1137.
47. L. Zhang and S. Jahanshahi: *The Seventh International Conference on Molten Slags, Fluxes and Salts*, 2004, pp. 51-56.
48. B.O. Mysen, F.J. Ryerson, and D. Virgo: *Am. Mineral*, 1980, vol. 65, pp. 1150-1165.
49. E.D. Grave, J.D. Sitter, and R. Vandenberghe: *Appl. Phys.*, 1975, vol.7, pp.77-80.
50. T. Ye, S. Li, X. Wu, M. Xu, X. Wei, K. Wang, H. Bao, J. Wang, and *J. Chen: J. Mater. Chemi. C*, 2013, vol. 1, pp. 4327-4333.
51. J.L. Li, Q.F. Shu, X.M. Hou, and K.C. Chou: *ISIJ Int*., 2015, vol. 55, pp. 830-836.
52. R.J. Kirkpatrick: *Am. Mineral.*, 1975, vol. 60, pp. 798-814.
53. K. Mills, L. Yuan, and R. Jones: *J. S. Afr. Insti. Min. Metall*., 2011, vol. 111, pp. 649-658.

Figures and Tables:

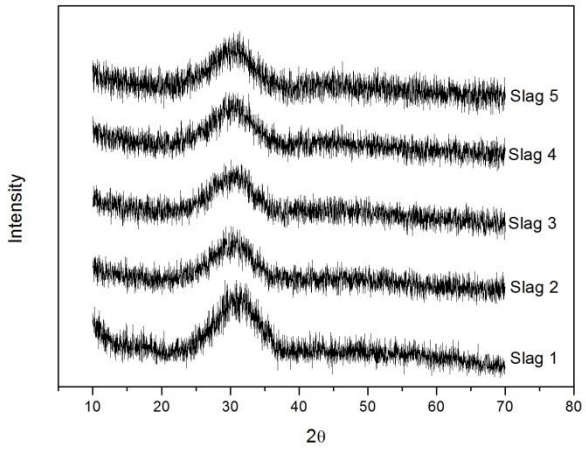

Figure 1 XRD patterns of different quenched slags at 1823K.

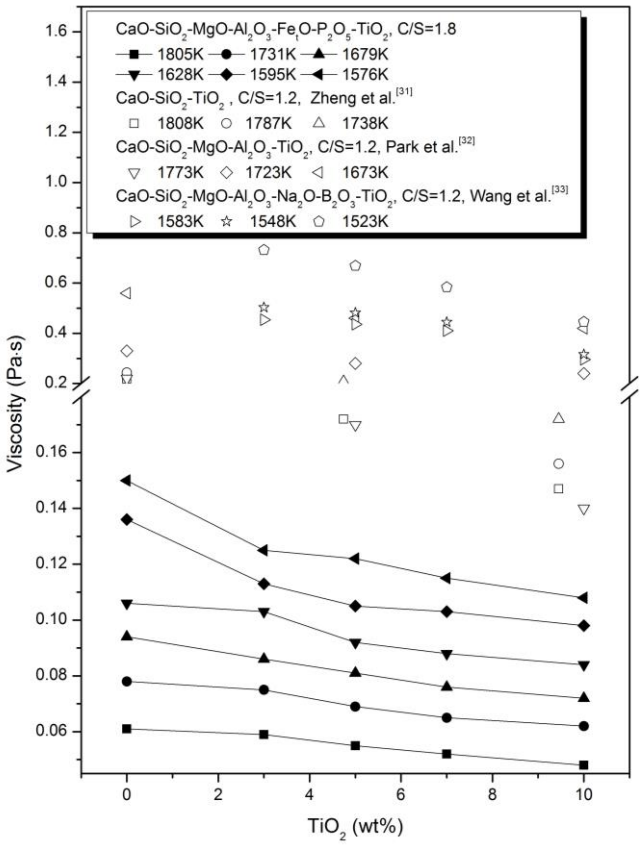

Figure 2 Effect of TiO_2 on the viscosity of CaO-SiO_2-MgO-Al_2O_3-Fe_tO-P_2O_5-(TiO_2) steelmaking slags.

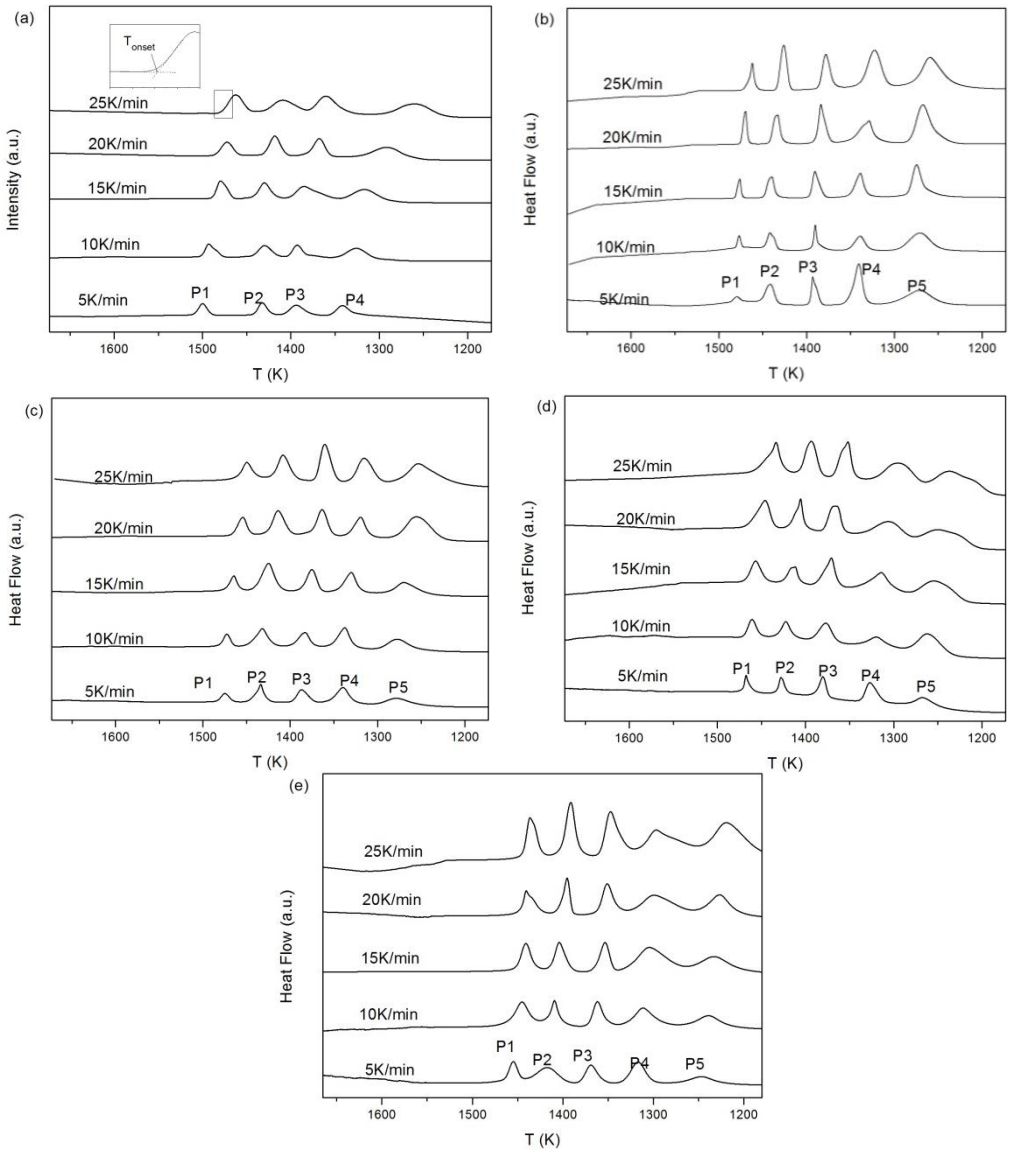

Figure 3 DSC curves of non-isothermal crystallization of slags at various cooling rates: (a) Slag 1, (b) Slag 2, (c) Slag 3, (d) Slag 4 and (e) Slag 5.

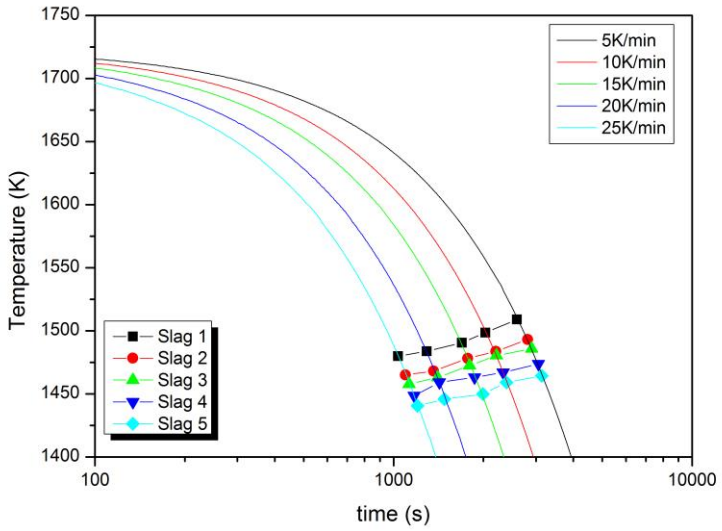

Figure 4 CCT diagrams of the primary crystal at different TiO_2 contents.

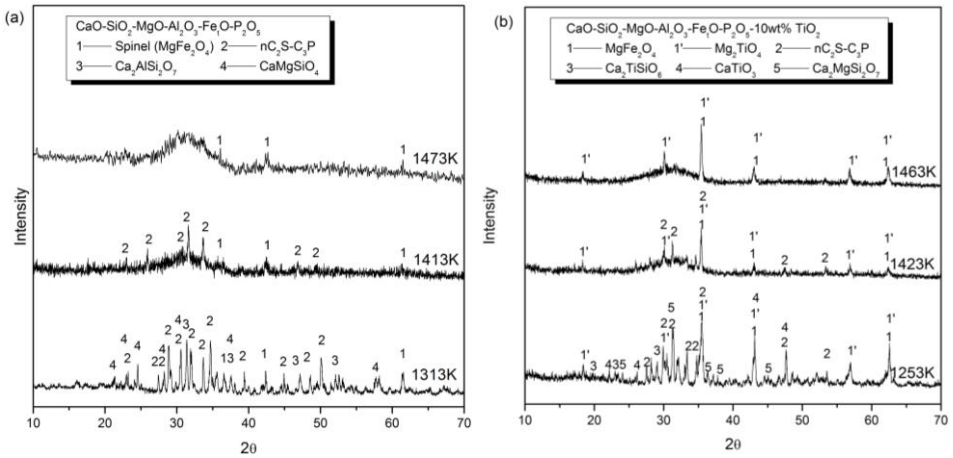

Figure 5 XRD results of slag 1 and slag 3 quenched at corresponding temperatures.

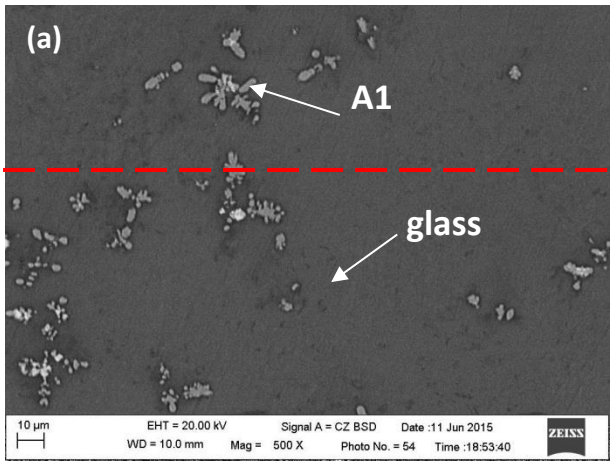
(a)
A1
glass
10 µm
EHT = 20.00 kV
WD = 10.0 mm
Signal A = CZ BSD
Mag = 500 X
Date :11 Jun 2015
Photo No. = 54
Time :18:53:40
ZEISS

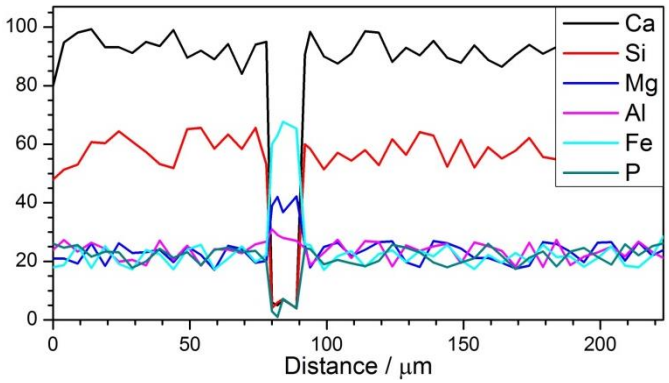
Ca
Si
Mg
Al
Fe
P
100
80
60
40
20
0
0
50
100
150
200
Distance / µm

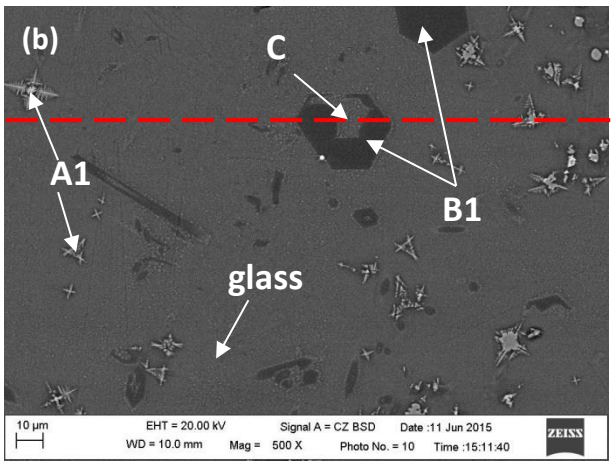
(b)
C
A1
B1
glass
10 µm
EHT = 20.00 kV
WD = 10.0 mm
Signal A = CZ BSD
Mag = 500 X
Date :11 Jun 2015
Photo No. = 10
Time :15:11:40
ZEISS

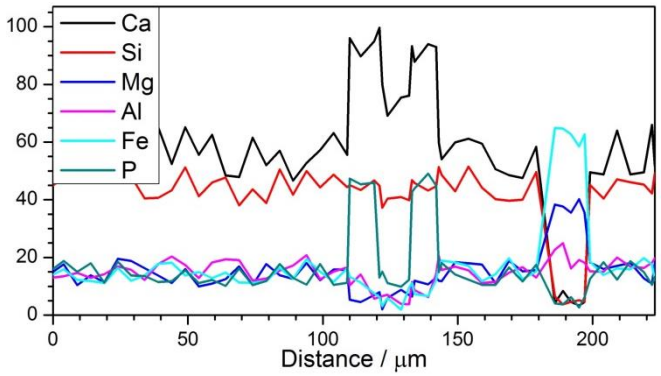
Ca
Si
Mg
Al
Fe
P
100
80
60
40
20
0
0
50
100
150
200
Distance / µm

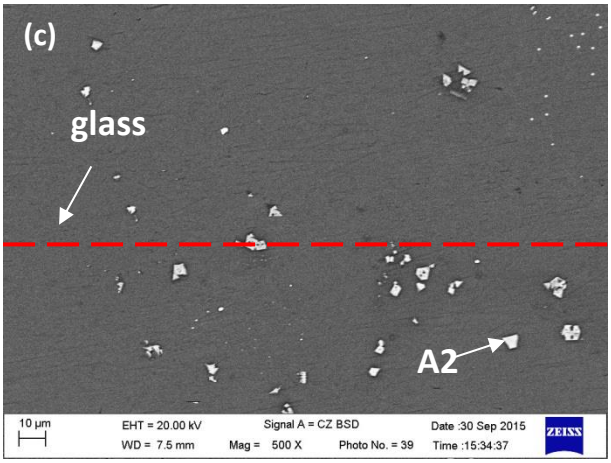
(c)
glass
A2
10 µm
EHT = 20.00 kV
WD = 7.5 mm
Signal A = CZ BSD
Mag = 500 X
Date :30 Sep 2015
Photo No. = 39
Time :15:34:37
ZEISS

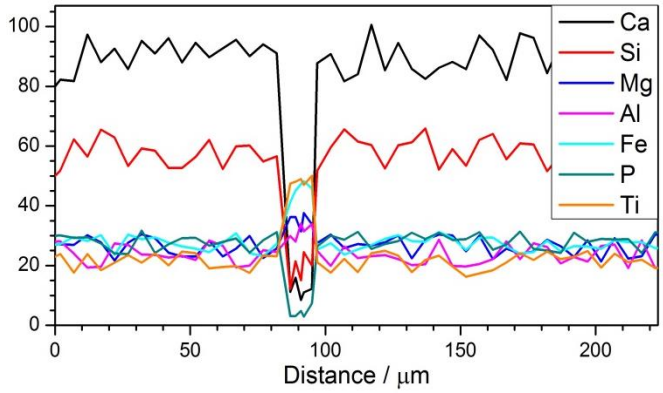
Ca
Si
Mg
Al
Fe
P
Ti
100
80
60
40
20
0
0
50
100
150
200
Distance / µm

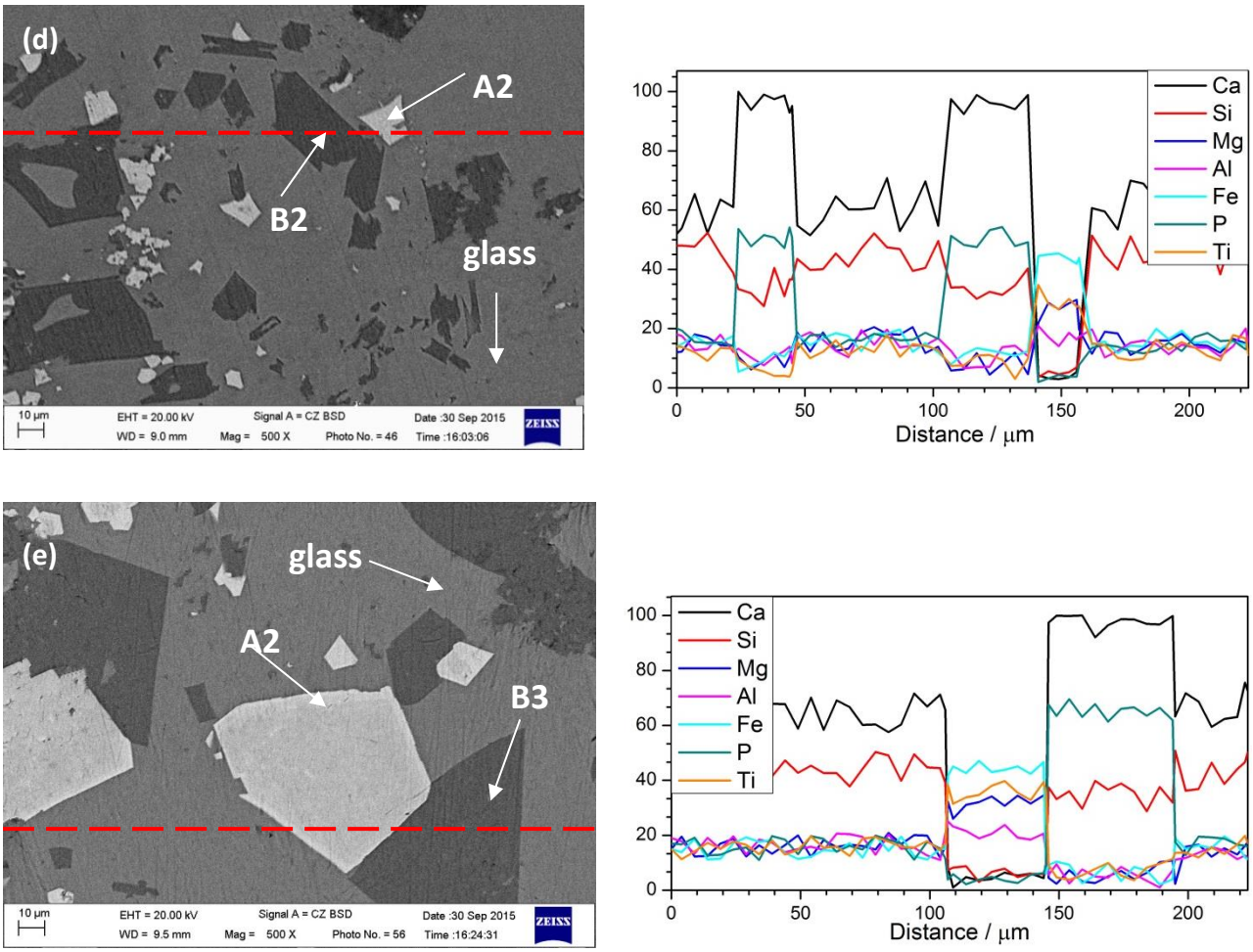

Figure 6 BSE images and EDS result of slags at the cooling rate of 10 K/min and quenched at corresponding temperatures: (a) Slag 1 (1473K), (b) Slag 1 (1413K), (c) Slag 3 (1573K), (d) Slag 3 (1473K) and (e) Slag 5 (1403K).

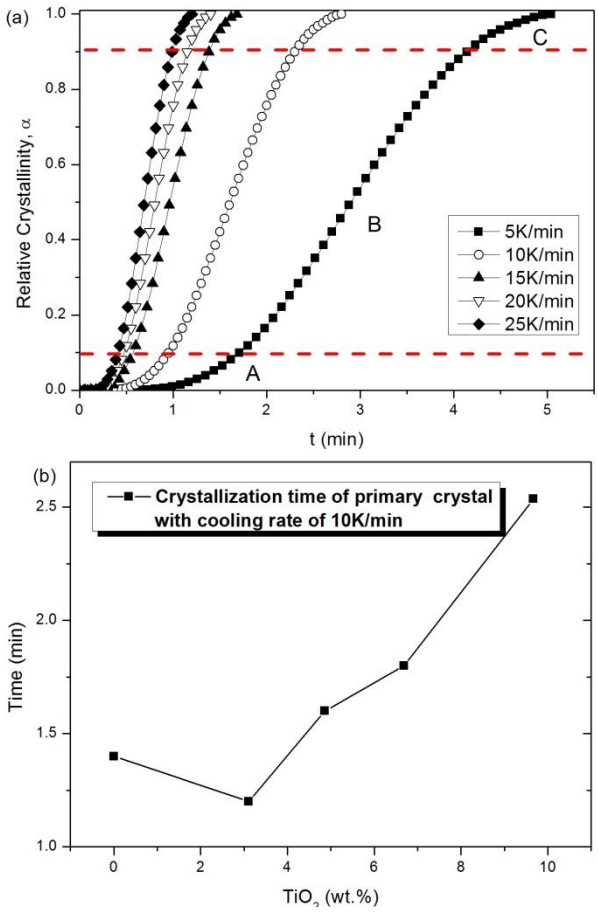

Figure 7 (a) Relative crystallization as a function of time for slag 1 at five different cooling rates; (b) Crystallization time of primary crystals with the cooling rate of 10K/min.

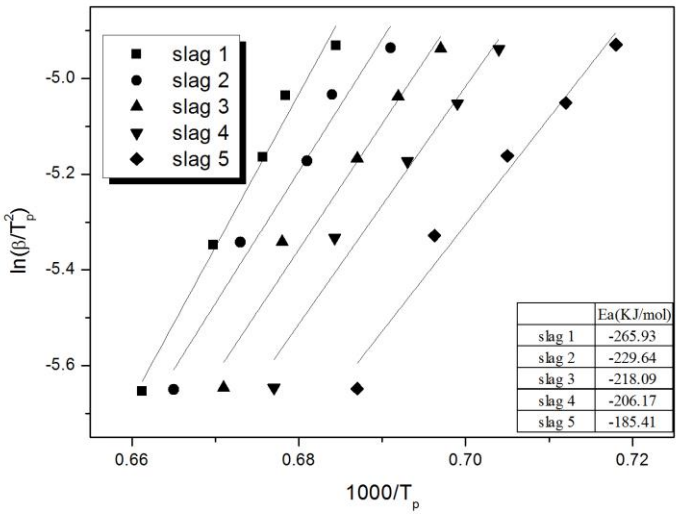

Figure 8 Kissinger plot for determination of the activation energy (Ea) for exothermal reaction of the primary crystal from DSC with different cooling rates (5, 10, 15, 20 and 25 K/min).

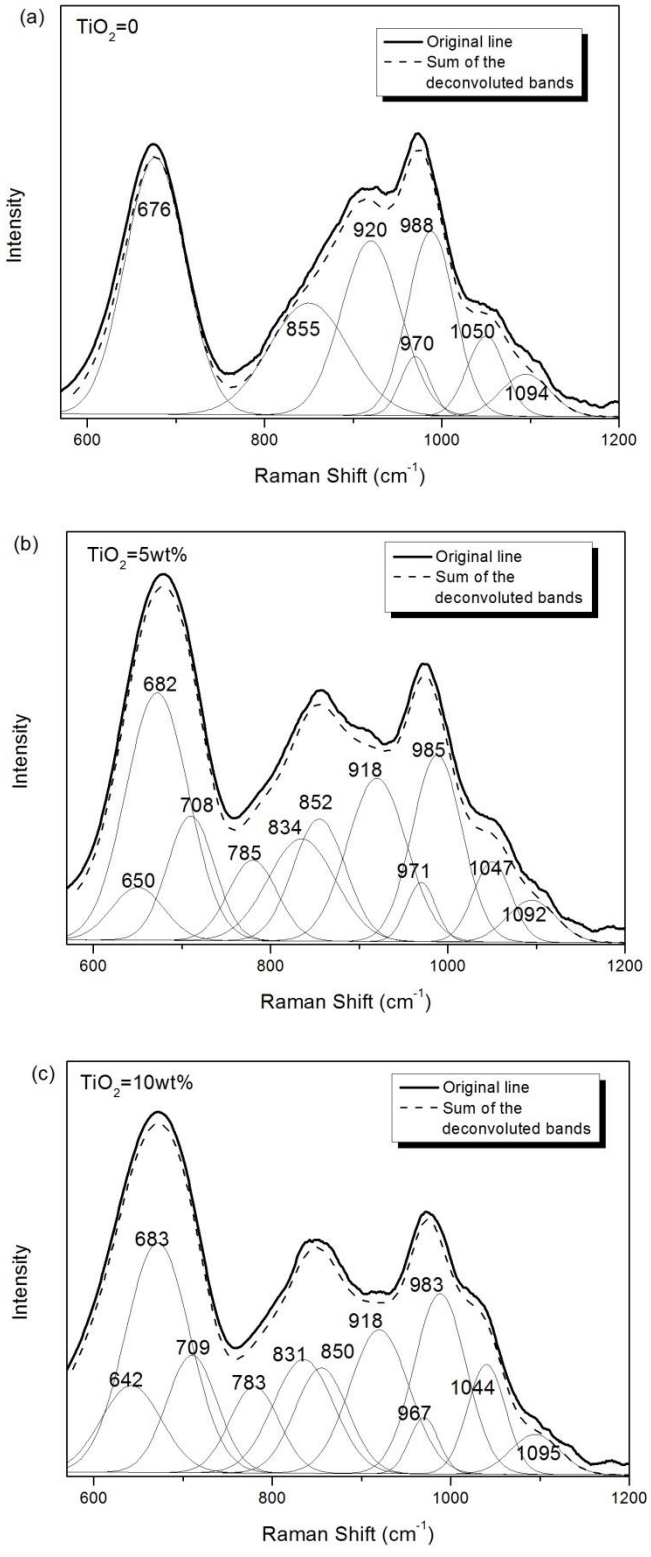

Figure 9 Deconvoluted Raman spectra of $CaO-SiO_2-MgO-Al_2O_3-FetO-P_2O_5-(TiO_2)$ slags with varying TiO_2 contents: (a) slag 1,(b) slag 3, and (c) slag 5.

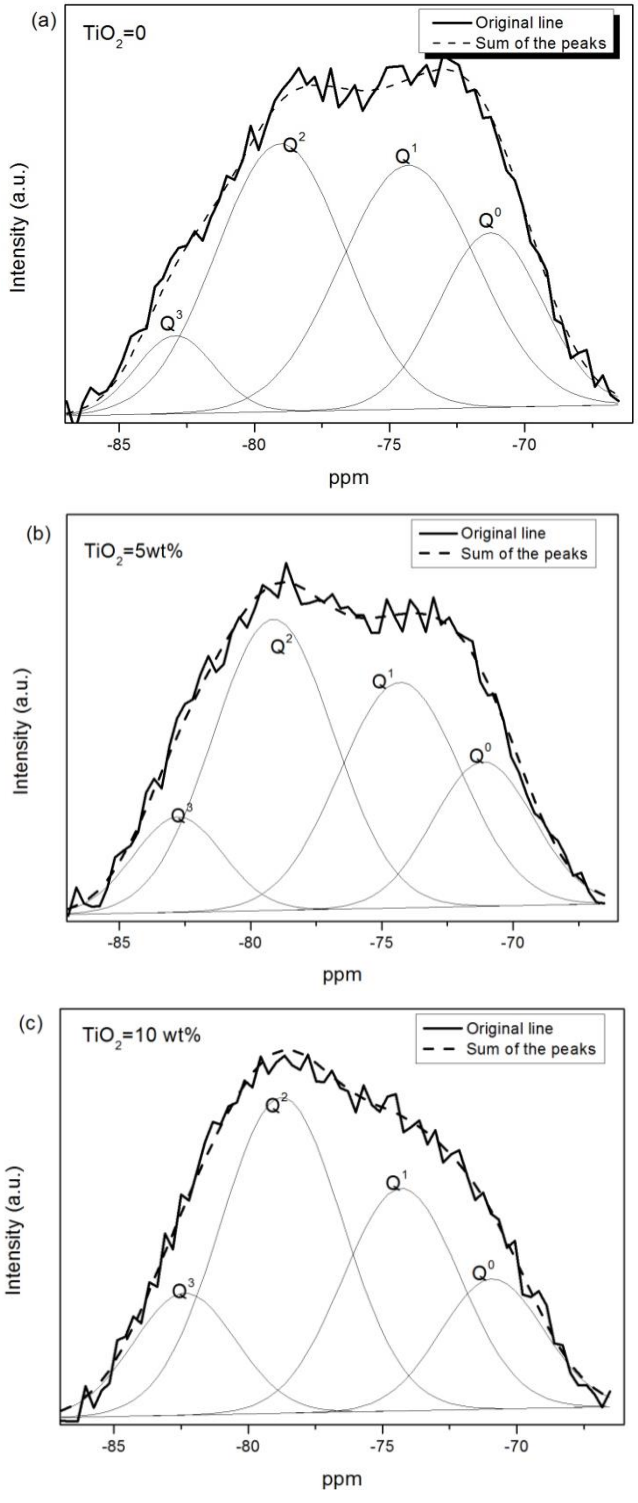

Figure 10 Deconvolved results of ^{29}Si MAS-NMR for slag with TiO_2 content of 0, 5 and 10wt%.

Table 1. Analyses result of synthesized slag compositions (wt.%).

Slag	Basicity	$Fe^{3+}/\sum Fe$	CaO	SiO_2	MgO	Al_2O_3	Fe_tO	P_2O_5	TiO_2
1	1.72	0.791	37.81	21.91	6.54	4.85	19.47	9.42	0
2	1.75	0.781	35.51	20.24	6.67	4.85	20.11	9.51	3.11
3	1.79	0.774	34.89	19.46	6.81	4.72	19.87	9.39	4.86
4	1.75	0.791	33.28	18.98	6.91	4.91	19.69	9.54	6.69
5	1.81	0.773	32.26	17.84	6.52	4.69	19.36	9.66	9.67

Table 2. Results of EDS analysis of P-enriched phase for slag 1, 3 and 5 shown in Figure 6 (wt.%).

Slag	P-enriched Phase	CaO	SiO_2	MgO	Al_2O_3	Fe_tO	P_2O_5	TiO_2
1	B1	54.11	19.64	2.45	2.71	3.17	17.92	0
3	B2	52.03	17.56	1.44	3.01	1.93	22.12	1.91
5	B3	47.66	16.03	1.78	0.91	2.11	30.17	1.34